ACS Catalysis

Research Article

Cite This: ACS Catal. 2018, 8, 3833−3843

pubs.acs.org/acscatalysis

Anion Resistant Oxygen Reduction Electrocatalyst in Phosphoric Acid Fuel Cell

Kara Strickland, Ryan Pavlicek, Elise Miner,[†] Qingying Jia, Ivo Zoller,[‡] Shraboni Ghoshal, Wentao Liang, and Sanjeev Mukerjee*

Department of Chemistry and Chemical Biology, Northeastern University Center for Renewable Energy Technology, 317 Egan Research Center, 360 Huntington Avenue, Boston, Massachusetts 02115, United States

Supporting Information

ABSTRACT: Phosphoric acid fuel cells are successfully used as energy conversion technologies in stationary power applications. However, decreased proton conductivity and lower oxygen permeability of phosphoric-acid-imbibed membranes require prohibitive loadings of the traditional noble-metal-based electrocatalyst, such as platinum supported on carbon. Additionally, specific adsorption of phosphate anions on the catalyst results in a surface poisoning that further reduces electrocatalytic activity. Here we report a nonplatinum group metal (non-PGM) electrocatalyst as an alternative cathode electrocatalyst for oxygen reduction in phosphoric acid fuel cells. The non-PGM was prepared in a one-pot synthesis using a metal organic framework and iron salt precursor. Phosphate anion poisoning was monitored electrochemically and spectroscopically in reference to the current state-of-the-art Pt-based catalyst at room temperature. Unlike Pt-based catalysts that are prone to phosphate poisoning, the non-PGM electrocatalyst exhibits immunity to surface poisoning by phosphate anions at room temperature. Imaging with microscopy reveals that the iron particles are isolated from the electrolyte by graphitic layers, which ultimately protect the iron from phosphate anion adsorption. The non-PGM electrocatalyst represents the highest performance to date in a high-temperature phosphoric acid membrane system, which is likely attributed to its immunity to phosphate adsorption at the harsher fuel cell environments.

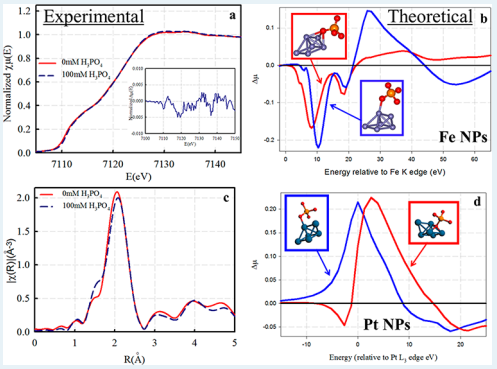

KEYWORDS: *phosphate poisoning, nonpgm catalysts, oxygen reduction, fuel cells, X-ray absorption spectroscopy*

1. INTRODUCTION

Development of environmentally friendly energy-conversion devices is a contemporary challenge facing scientists, and fuel cell technologies are promising candidates due to their high theoretical energy density. Phosphoric acid fuel cells (PAFC) were one of the first commercially viable fuel cell technologies and are currently used for stationary power applications in multiple countries.[1−3] The PAFC technology employs a concentrated phosphoric acid (85−100 wt % H_3PO_4) electrolyte that allows operation in the range of 150 to 220 °C, which overcomes problems of the lower temperature polymer electrolyte fuel cells (PEMFCs, typically based on perfluorinated sulfonic acid such as Nafion, Dupont, U.S.A.). The latter being reliant on proper membrane hydration for proton conductivity and hence limited to below 100 °C (typically 80 °C) with concomitant challenges of exponentially higher susceptibility to poisoning (such as CO, S, and halides[4]), mandating therefore a much larger balance of plant as compared to PAFC operating temperatures. In addition, the ability to use the waste heat of a PAFC results in a higher overall efficiency (total combined heat and power (CHP) efficiency typically in the range 80%, based on higher heating value (HHV) of H_2) compared with 65−70% for PEMFCs.[2]

Current state of the art in PAFCs has transitioned to phosphoric acid (PA)-imbibed membrane systems replacing the earlier silicon carbide matrix based membrane electrode assemblies (MEAs). Best known membranes based on polybenzimidazole (PBI) and its analogues[5−9] have emerged in the past decade, exhibiting high proton conductivity (150−200 °C), low gas permeability, excellent thermal stability, and a nearly zero water drag coefficient. Some of the drawbacks of these polymer systems such as moderate mechanical properties, especially in case of those containing low-molecular weight fractions,[10,11] have been addressed with modification in polymer chemistry and processing[12,13] as well as alternative polymer membranes such as those based on poly ether sulfone based copolymers containing pyridine and tetramethyl biphenyl groups.[14−16] For amphoteric anions such as dihydrogen phosphate conductivity is expected to increase monotonically with acid concentration, typical doping levels in membranes are in the range of 300 wt %,[15] which provides for a mechanically robust single phase polymer film amenable for bonding to electrodes and MEA fabrication.

Received: January 29, 2018
Revised: March 6, 2018
Published: March 27, 2018

DOI: 10.1021/acscatal.8b00390
ACS Catal. 2018, 8, 3833−3843

Conventional expectation of enhanced kinetics at the typical elevated temperature of operation (150−220 °C) for PAFCs compared to PEMFCs predominantly as a result of the higher collision frequency is largely negated by the specific adsorption of phosphate anions (dihydrogen phosphate) and associated surface poisoning of most supported electrocatalyst such as Pt/C. Detailed aspect of such poisoning has been reported by us[17,18] and others[19] in prior reports. Briefly, this anion poisoning in acidic pH is specially manifest at potentials positive to that corresponding to potential of zero and is well reported using radio tracer studies.[20] In addition, the 1 order of magnitude lower proton conductivity in PA imbibed membranes (150−200 °C) and approximately 4- to 5-fold lower oxygen permeability as compared to typical PEMFCs (i.e., Nafion type) results in relatively lower power density (typically in the range of 140−150 mW/cm^2 compared to 800−1000 mW/cm^2 at 0.7−0.65 V). These drawbacks exacerbate the key barrier for wide application of this CHP technology, which is principally related to the cost of the catalysts in terms of the noble metal loading. Considering the typical Pt loading in PA imbibed systems to be between 1.5 and 3.0 mg (Pt)/cm^2 (MEA), we have a requirement of 11−20 g (Pt)/KW. Contrast this with the current approximate loading of 0.25−1.1 g(Pt)/KW at ≥0.65 V vs RHE for a lower temperature PEMFCs (typically 80 °C) thus representing a 10- to 20-fold loading difference between the two types of fuel cell technologies. As a result for PAFCs, typical cost of noble metals/KW for PA imbibed membrane systems is in the range of $ 550−1000/KW, which is unsustainable.

Herein we report a significant breakthrough, overcoming this key barrier related PAFCs MEA and stack cost via elimination of noble metals at the cathode electrode interface. This is achieved using a recently reported[21] unique nonplatinum group metal (non-PGM) electrocatalyst prepared using metal organic framework (MOF) precursors (hereto referred to as FePhen@MOF-ArNH$_3$). This electrocatalyst is one of the first confirmed representations of an active site with no direct evidence of Fe−N$_x$ coordination; instead the structure consists of embedded Fe−Fe$_x$C nanoparticle moieties in a carbo-nitrided nanofiber matrix. The vast wealth of recent reports on non-noble-metal electrocatalyst prepared using precursors in conjunction with metal salts and carbon support (template or nontemplated) involve direct coordination of transition metal with nitrogen in addition to embedded transition-metal nanoparticles in their close proximity (see reference).[22,23] Preliminary studies of non-PGM electrocatalysts suggest that the ORR activity of Fe-based non-PGMs are resistant to anion poisoning in a variety of electrolytes.[24,25] A recent non-PGM study specific to phosphate poisoning used electrochemical measurements conducted at room temperature to show improved phosphate tolerance of a Fe−N$_x$-based electrocatalysts when compared to Pt/C.[26] However, the source of phosphate anion tolerance on Fe-based non-PGM electrocatalysts and their ability to withstand the operating temperature and environment of HT-PEM fuel cells has not been addressed.

This study investigates the use of a MOF-supported Fe-based non-PGM (FePhen@MOF-ArNH$_3$) as an alternative ORR electrocatalyst in HT-PEM fuel cells. Preliminary tests of FePhen@MOF-ArNH$_3$ showed very little activity loss in the presence of phosphoric acid when compared with its Pt-based counterpart.[27,28] Physical characterization elucidated the make-up and morphology of the material and electrochemical testing monitored the kinetics of ORR in the presence of varied concentrations of phosphoric acid. In addition, in situ XAS was used to monitor how the electronic and structural properties of the Fe present in FePhen@MOF-ArNH$_3$ are changed under the operating electrochemical environment with and without the presence of phosphoric acid. The $\Delta\mu$ technique[29,30] was applied to investigate changes in adsorbate coverage as a function of potential in order to understand the interaction of the phosphate anions with the surface of FePhen@MOF-ArNH$_3$. All of these results are compared with Pt/C (Tanaka, Japan) as a reference standard.

2. METHODS

2.1. Catalyst Synthesis. The commercial Pt/C (46%) electrocatalyst was obtained from Tanaka Kikinzoku (Japan). For the synthesis of FePhen@MOF, previously published with quantities specified,[21] 2-methylimidazole was dissolved in methanol at room temperature with stirring. In a separate flask, zinc(II) nitrate χ-hydrate and 1,10-phenanthroline monohydrate were dissolved in methanol and water at room temperature with stirring. Once both flasks' contents were fully dissolved, they were mixed. Iron(II) acetate was added to the reaction, and this was stirred at room temperature for 24 h. Progress of the reaction is evident from the increased turbidity of the solution and appearance of pale orange color. The formed suspension was centrifuged at 4000 rpm for 25 min and washed 3 times with methanol; each washing step consisting of centrifugation at 3700 rpm for 17 min. The resulting orange/white solid was dried in a vacuum oven for 6−12 h at 60−70 °C and afforded formation of the desired FePhen@MOF, a light tan powder. The dried powder was then subjected to either one or two heat-treatments (i.e., in argon at 1050 °C with a 1 h dwell time (FePhen@MOF-Ar) and ammonia at 1050 °C with an 18 min dwell time (FePhen@MOF-ArNH$_3$), respectively). Perchloric acid electrolyte was prepared using double-distilled 70% perchloric acid (GFS Chemicals). The phosphoric acid (H_3PO_4, 85%, Alfa Aesar) was purified following a standard procedure described in the literature.[31]

2.2. Electrochemical Characterization. Electrochemical measurements were carried out on glassy carbon (GC) disk (5.61 mm diameter, Pine Instruments) that was polished with 0.05-μm alumina paste (Buehler, Lake Bluff, IL) and then sonicated in distilled water and isopropyl alcohol. Catalysts inks were prepared by dispersing the catalyst in a volume of 1:1 Millipore water/isopropyl alcohol with 10 vol % of 5 wt % Nafion as a binder. The ink solution was then sonicated approximately 30 min to get a uniform suspension. A small volume of the catalyst ink was deposited on the GC substrate to obtain a platinum metal loading of 15 μg/cm^2 and a NPMC loading of 600 μg/cm^2. All electrochemical measurements were carried out at room temperature (20−25 °C) in a standard electrochemical cell (Chemglass) with an acid electrolyte using a rotating disk electrode (RDE) setup from Pine Instrument Company connected to an Autolab bipotentiostat (PGSTAT302N). Cyclic voltammetry was run on both Pt and non-Pt catalysts in 0.1 M perchloric acid ($HClO_4$) purged with argon. ORR was investigated by the RDE technique after oxygen purge in the 0.1 M $HClO_4$ solution followed with incremental addition of 1, 10, and 100 mM phosphoric acid (H_3PO_4). Scans were recorded at 20 mV/s and all potentials are referenced to a reversible hydrogen electrode (RHE) scale made from the same solution as the electrolyte.

2.3. Electrode and MEA Fabrication, Testing Procedures. Aqueous catalysts inks composed of FePhen@MOF-

DOI: 10.1021/acscatal.8b00390
ACS Catal. 2018, 8, 3833−3843

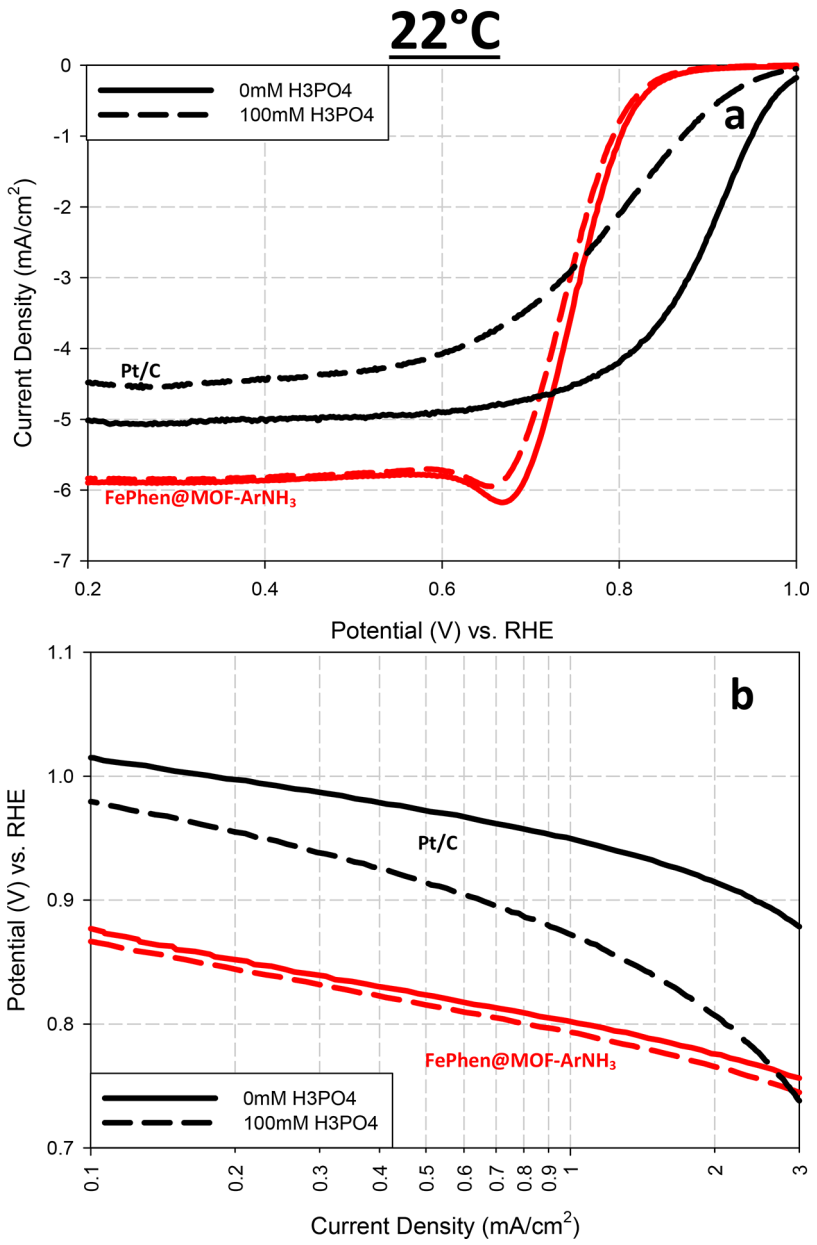

Figure 1. RRDE electrochemical performance. (a) Rotating disk electrode (RDE) ORR polarization plots collected with FePhen@MOF-$ArNH_3$ and Tanaka Pt/C in O_2 saturated electrolyte (0.1 M $HClO_4$) with/without 100 mM H_3PO_4 at 20 mV/s with rotation rate of 1600 rpm at room temperature (22 °C). (b) Mass-transport corrected Tafel plots of FePhen@MOF-$ArNH_3$ and Tanaka Pt/C in O_2 saturated electrolyte (0.1 M $HClO_4$) with and without 10 mM H_3PO_4 at 20 mV/s and 1600 rpm at room temperature.

$ArNH_3$, PTFE, water, isopropyl alcohol, and proprietary (Advent Technologies, GR) additives were prepared. These proprietary additives are primarily used for ink stabilization. Inks were coated onto a commercial GDL (NuVant LT1400) using a draw-down technique (Elcometer 4340) until catalyst loading reached 2 mg/cm^2 (determined through incremental weighing of the electrode). Anodes were commercial Advent A1100W Pt GDE (1.0 mg_{Pt}/cm^2), while the membranes were polybenzimidazole (PBI)-based. Electrodes were individually hot-pressed to Kapton-based subgaskets, and then both electrodes were hot-pressed with membrane using procedures provided by Advent Technologies. Following a final drying step of the MEA, testing was done in standard Fuel Cell Technologies hardware (5 cm^2). MEAs were tested on home-built stations, with polarization curves being collected using an HP 6050A load supply and LabView software. *iR*-corrected Tafel plots for oxygen testing were generated using the high-frequency resistance (HFR) from electrochemical impedance spectroscopy (EIS). EIS was collected on a Metrohm Autolab (PGSTAT302N) with a 20A current booster (PGSTAT30) and associated Nova software. EIS spectra were composed of 50 data points from 20 MHz to 100mHz (logarithmic scale) and taken potentiostatically at a series of potentials over the operational range of the fuel cell.

2.4. X-ray Absorption Spectroscopy (XAS) Measurements. The in situ XAS studies at the Fe K-edge (7112 eV) were performed at X3B beamline of National Synchrotron Light Source (NSLS, Brookhaven National Laboratory, NY). A specially designed spectro-electrochemical cell was utilized and has been described previously.[32] The Fe K-edge spectra were

DOI: 10.1021/acscatal.8b00390
ACS Catal. 2018, 8, 3833−3843

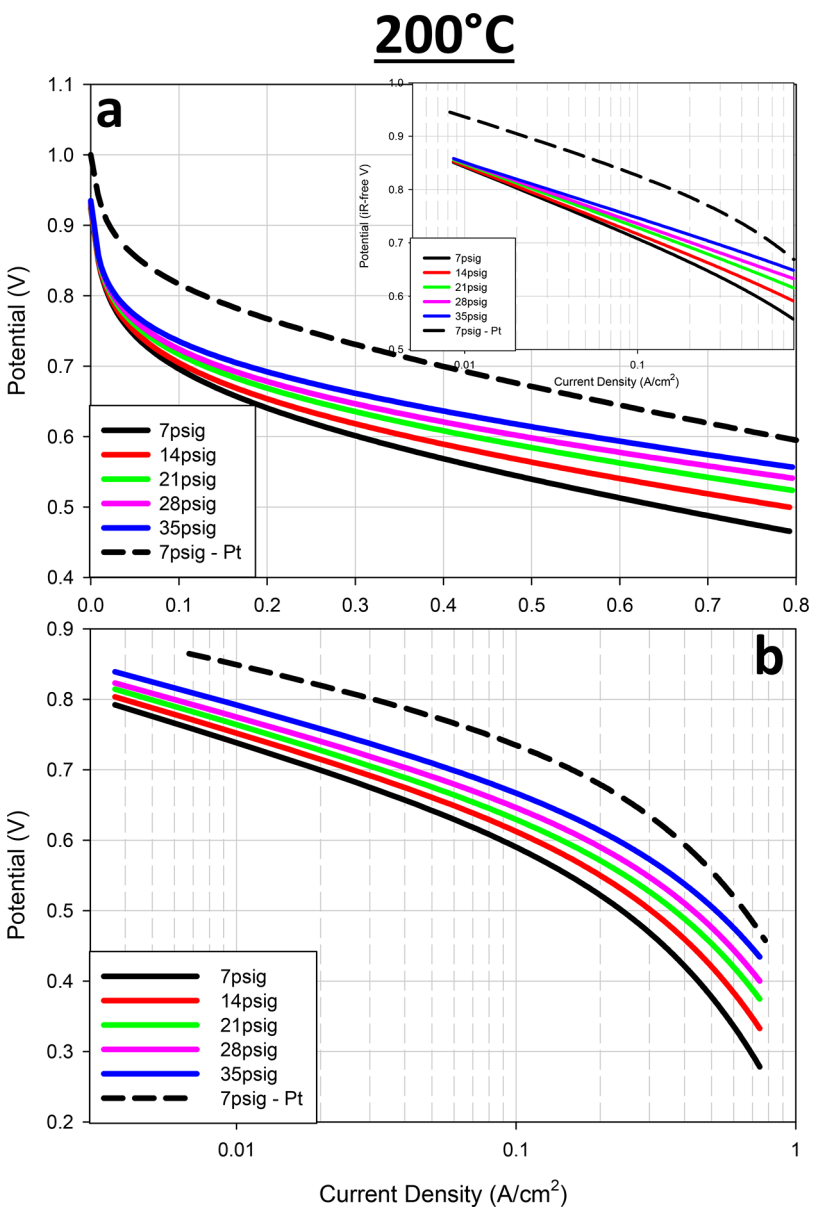

Figure 2. HT-PEMFC performance: (a) H_2/O_2 fuel cell polarization curve for a non-PGM FePhen@MOF-ArNH_3 cathode (1.95 mg/cm^2 loading) as a function of backpressure. Insert: *i*R-corrected Tafel plot. (b) H_2/air fuel cell polarization curve for the same MEA as (a). Pt data at 7 psig in O_2 and air included for comparison. Full Pt data sets can be found in the Supporting Information.

collected in fluorescence mode with a 32-element Ge solid state detector as a function of potential in the range 0.1−0.9 V vs RHE. All testing was done at room temperature given the limitations of operating at the beamline. A pseudo steady state was established by holding the cell for approximately 5 min before collecting the spectra. The electrolyte, 0.1 M $HClO_4$, was saturated with either argon or oxygen. Athena[33] and Artemis[34] programs were used to process and fit the data. IFEFFIT suite[35] was used to calibrate, align, and normalize the scans. FEFF6 code[35] was used to calculate scattering paths to model the χ(R) transforms. Delta-Mu ($\Delta\mu$) analysis of the Fe K-edge followed specific normalization procedures that are described in the literature.[36] Difference spectra were obtained by utilizing the eq 1 where μ(V, Ar 100 mM H_3PO_4) represents the XANES of the catalyst at various potentials in Ar saturated 0.1 M $HClO_4$ electrolyte doped with 100 mM H_3PO_4 and the reference, μ(0.3 V, Ar) comprising XANES at 0.3 V in Ar-saturated 0.1 M $HClO_4$ electrolyte sans H_3PO_4. FEFF8 code[36] was used to generate theoretical delta mu curves ($\Delta\mu$t) using the relationship

$$\Delta\mu t = \mu(PO_4 ads - Fe_6) - \mu(Fe_6) \quad (1)$$

where the adsorbate is in a specific binding site on Fe.

3. RESULTS

3.1. Electrochemical Performance. A commercially available Pt/C electrocatalyst (46% Pt/C, average particle size 15 Å, Tanaka, Japan) was used as a reference material in this study to estimate the poisoning effect of phosphoric acid on FePhen@MOF-ArNH_3. Adsorption of anions such as phosphate on this reference standard have been well characterized[17,18] together with its associated increase in overvoltage for ORR. In consonance with these prior studies, comparative study of the effect of phosphate anion poisoning in terms of

DOI: 10.1021/acscatal.8b00390
ACS Catal. 2018, 8, 3833−3843

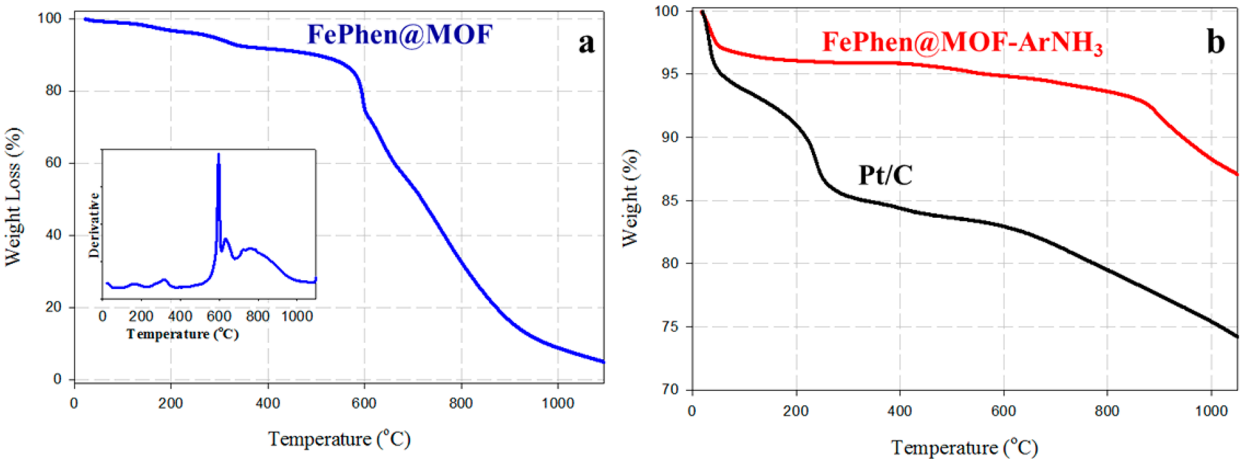

Figure 3. Thermogravimetric analysis. (a) Thermogravimetric analysis of FePhen@MOF with inset of derivative plot. (b) TGA analysis of heat treated FePhen@MOF-ArNH$_3$ and Tanaka Pt/C.

kinetic parameters of ORR, using a rotating disk electrode (RDE) technique, was performed in 0.1 M $HClO_4$ with incremental doses of phosphoric acid (0−100 mM H_3PO_4, Supporting Information, Figure S1). Based on dissociation constants of polyprotic phosphoric acid the predominant species at pH 1 is $H_2PO_4^-$ (comparatively the concentration of HPO_4^{2-} is 6 orders of magnitude less than $H_2PO_4^-$at room temperature, and even higher at higher temperatures given the effect of temperature on the dissociation constant of exothermic and endothermic reaction, respectively). Comparison of Pt/C with the MOF-derived catalyst hereto referred to as FePhen@MOF-ArNH$_3$ (see below for structural and synthesis information) in 0.1 M $HClO_4$ and 1600 rpm are shown in Figure 1a at two different concentrations of H_3PO_4 (0 and 10 mM). As evident from the data represented in the Supporting Information Figure S1, concentrations beyond 10 mM do not cause significant changes to the observed overvoltage for ORR on supported catalyst such as Pt/C. This limit of concentration dependence is of course dictated by surface area and availability of the more susceptible Pt (111) surface. Each RDE profile comprises of three regions: (1) diffusion controlled region (<0.7 V), (2) mixed diffusion-kinetic region (0.7 to 0.9 V for Pt/C and 0.7 to 0.8 V for FePhen@MOF-ArNH$_3$), and (3) the kinetic region (>0.9 V for Pt/C and >0.8 V for FePhen@MOF-ArNH$_3$). As can be seen in the kinetic region of Pt/C (Figure 1a) in 0 mM H_3PO_4 the on-set of ORR is ∼1.0 V vs RHE, and a well-defined limiting current is established in the diffusion controlled region. The diffusion-limiting current (i_{lim}) is defined by the Levich equation:

$$i_{lim} = 0.62nFD^{2/3}\nu^{-1/6}C_O \quad (2)$$

where n is the number of electrons transferred, F is the Faraday constant, D is the diffusion coefficient of O_2 in 0.1 M $HClO_4$, ν is the kinematic viscosity, and C_O is the concentration of O_2 in the electrolyte. Introduction of just 10 mM H_3PO_4 into the electrolyte causes a slight decrease in the magnitude of the limiting current, which indicates that O_2 is being inhibited from reaching the electrode surface. Furthermore, when compared with the profile in the absence of H_3PO_4 the half-wave potential ($E_{1/2}$), a pseudo kinetic parameter characteristic of ORR activity, is shifted cathodically ∼150 mV (0.87 vs 0.72 V). Tafel plots derived from these polarization data provide further insight on the kinetic effect of adsorption of the phosphate anion (Figure 1b). Even though Tafel slopes are often used as an indicator of mechanistic changes, its use in such supported nanostructures such as Pt/C and especially on single-atom-coordinated structures represented by FePhen@MOF-ArNH$_3$ may stretch the limits of such interpretations. Mass-transport corrected kinetic currents using the well-known equation

$$i_k = i_{lim}xi/(i_{lim} - i) \quad (3)$$

where i_k represents the kinetic current density, i_{lim} is the diffusion limiting current density from eqn 1, and i is the current measured from ORR, provides a convenient method of comparing relative activity losses as a result of phosphate anion poisoning. Pt/C in the presence of 10 mM H_3PO_4 does indicate a significant increase of overvoltage in the Tafel performance (∼140 mV at 1−5 mA/cm^2) including a change in slope; concomitantly, the relative effect on FePhen@MOF-ArNH$_3$ is negligible (∼less than 3 mV) (Figure 1b), both exhibiting approximately similar limiting currents with and without the presence of phosphate anions. These results clearly show that the active sites of FePhen@MOF-ArNH$_3$ are not poisoned by phosphoric acid.

3.2. HT-PEMFC Performance. The natural tolerance of FePhen@MOF-ArNH$_3$ (like other F−N−C and M−N-C catalysts) to phosphate anion poisoning exhibited by RDE measurements (Figure 1a) encouraged us to implement the single HT-PEM steady-state fuel cell measurements (Figure 2a,b) at harsher conditions to examine its potential replacing Pt in practical applications. Polarization curves were collected at 200 °C at various backpressures on a 5 cm^2 membrane electrode assembly (MEA), using both oxygen and air as cathode fuel. While these results are still lower than Pt standard data also acquired (Supporting Figure S3a,b), they represent the highest published performance to date of non-PGM materials in HT-PEMFC environment. In looking at the data compared to the Pt reference data (Supporting Information), one thing noted is that the oxygen gain, the difference between oxygen and air data at identical testing conditions (200 mA/cm^2, 7 psig for example) is larger for the non-PGM catalyst (120 mV) than for the Pt data (85 mV). This implies that transport effects are part of the reason for the lower performance. Given the thicker non-PGM layer in these electrodes, these are issues that are going to be more prevalent while using non-PGM materials. However, these are also issues

DOI: 10.1021/acscatal.8b00390
ACS Catal. 2018, 8, 3833−3843

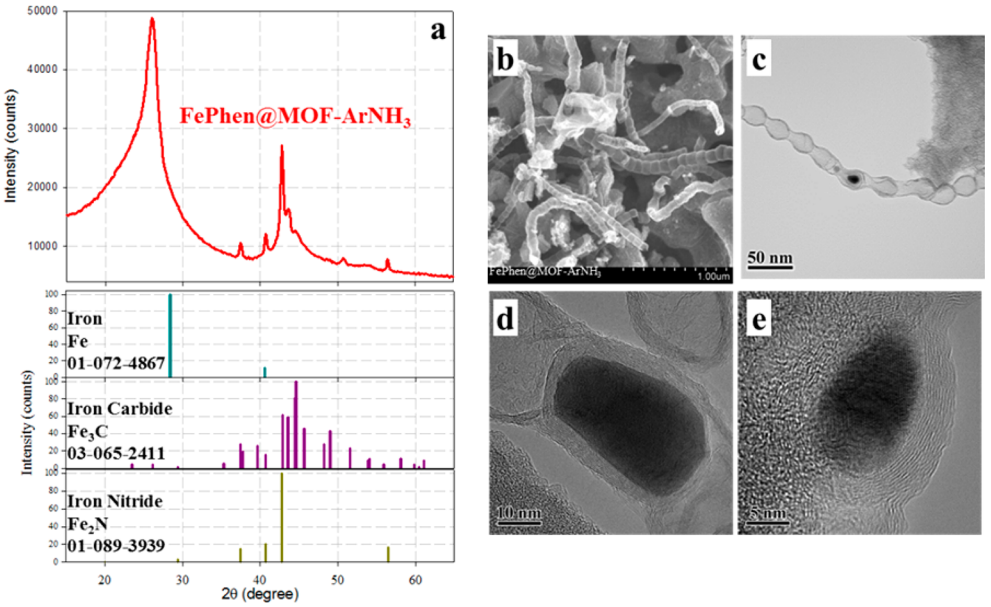

Figure 4. Physical characterization. (a) X-ray diffraction pattern (XRD) of FePhen@MOF-ArNH$_3$ and diffraction patterns of iron, iron carbide and iron nitride. (b) Scanning electron microscope (SEM) image of FePhen@MOF-ArNH$_3$, scale bar 1 μm. (c) Transmission electron microscope (TEM) image of bamboo-jointed CNT, scale bar 50 nm. (d) HR-TEM image of Fe/Fe$_3$C nanoparticle encapsulated in bamboo-joint of CNT in FePhen@MOF-ArNH$_3$, scale bar 10 nm. (e) HR-TEM image of Fe/Fe$_3$C nanoparticle surrounded by graphitic layers, scale bar 5 nm.

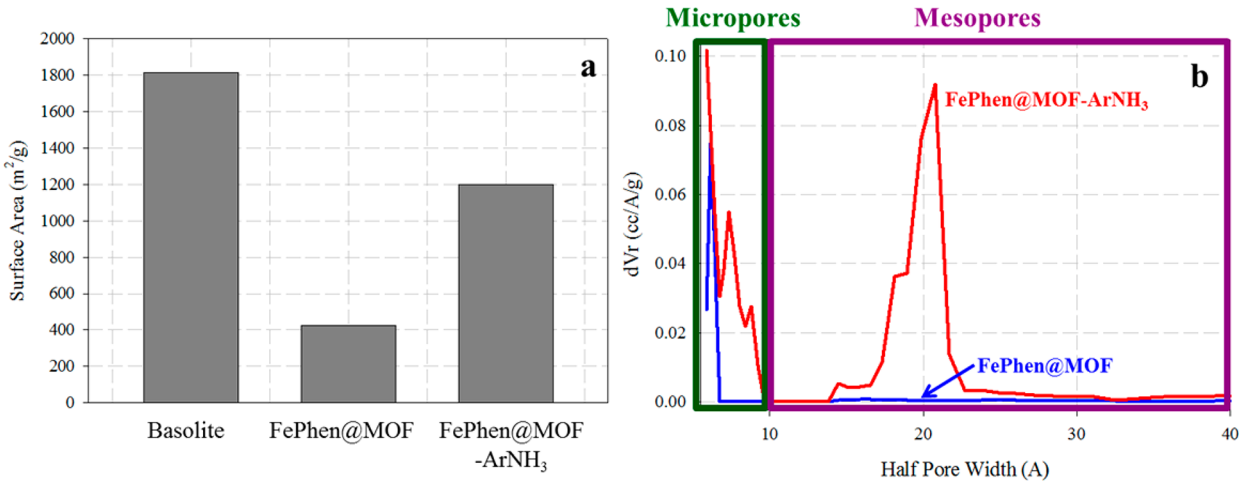

Figure 5. N_2 sorption analysis. (a) Bar graph plot of Brunauer–Emmett–Teller (BET) surface area of Basolite, FePhen@MOF, and FePhen@MOF-ArNH$_3$. (b) Pore volume as a function of half pore width of FePhen@MOF and FePhen@MOF-ArNH$_3$ using DFT method of split pore model.

that can be addressed through further studies on electrode formulation, including optimization of the PTFE content, and the use of a thinner base GDL. These results embolden the opportunity to replace Pt/C catalysts in HT-PEMFC technologies utilizing phosphoric acid electrolyte and compels further understanding of the source of ORR activity with FePhen@MOF-ArNH$_3$ in phosphoric acid.

3.3. Physicochemical Characterization. The as synthesized FePhen@MOF (see Methods section for synthesis) material was subjected to two heat treatments, first in argon at 1050 °C followed by ammonia at 1050 °C, to engender electrical conductivity and ORR activity. Thermogravimetric analysis (TGA) performed on FePhen@MOF (Figure 3a) reveals a gradual weight loss (35–350 °C) because of loss of guest species (H_2O and CH_3OH < 100 °C) followed by a small mass loss above 350 °C possibly due to the decomposition of some free 1,10-phenanthroline. The mass loss plateaus until 550 °C is reached, and a steep drop signifies the decomposition of the MOF framework[37] and eventual evaporation of Zn around 900 °C. The TGA conditions simulate the heat treatment in argon, hence we believe the resultant catalyst is a porous graphitic framework formed from the decomposition of the MOF support in which the Fe is retained and the Zn is lost through evaporation. The additional heat treatment in ammonia is known to introduce nitrogen functionalities and etch the amorphous carbon.[38]

An additional TGA analysis of the final electrocatalyst, FePhen@MOF-ArNH$_3$ (Figure 3b), revealed remarkable thermal stability at the elevated temperatures that is required for operation of HT-PEM fuel cells. FePhen@MOF-ArNH$_3$ shows a small drop in mass below 100 °C due to evaporation of water followed by a long plateau from 100 to 900 °C. The TGA trace of Pt/C is also characterized by water evaporation below 100 °C, but it is followed by a drop in mass from 200 to 250 °C

DOI: 10.1021/acscatal.8b00390
ACS Catal. 2018, 8, 3833–3843

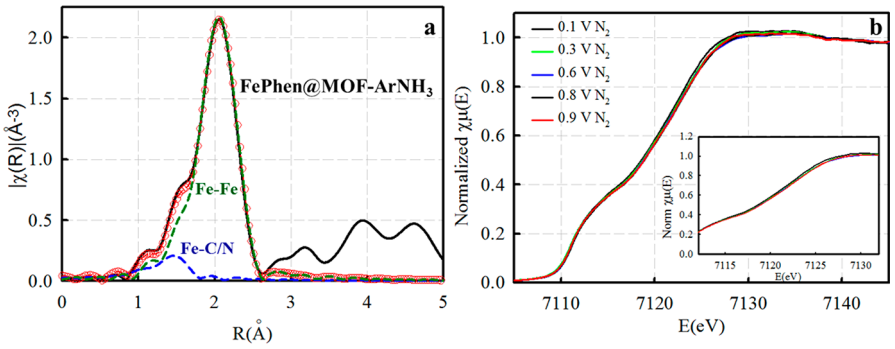

Figure 6. XAS characterization. (a) Fourier transform EXAFS of FePhen@MOF-ArNH$_3$ in N$_2$ saturated 0.1 M HClO$_4$ held at 0.3 V vs RHE. (b) Potential dependent normalized Fe K-edge XANES of FePhen@MOF-ArNH$_3$ collected in N$_2$ saturated 0.1 M HClO$_4$.

that is not witnessed with FePhen@MOF-ArNH$_3$. A possible source of mass loss at this temperature range could be attributed to the degradation of the O functional groups on the carbon.[39] FePhen@MOF-ArNH$_3$ compared to Pt/C displayed exceptional thermostability and maintained 90% of its original mass up to 950 °C (Figure 3b), as opposed to Pt/C which only maintained 90% of its original mass up to ∼200 °C.

In order to understand the source of thermal stability, powder X-ray diffraction (PXRD) was performed on FePhen@MOF-ArNH$_3$ to identify crystalline phases that were present following the two heat treatments. The PXRD pattern of FePhen@MOF-ArNH$_3$ (Figure 4a) reveals diffraction lines of graphite and several metallic iron phases (iron-Fe ($Im\bar{3}m$), iron carbide-Fe_5C_2 (C2/C), and iron nitride-Fe_2N ($P\bar{3}1m(162)$). Scanning electron microscopy (Figure 4b) revealed numerous bamboo-shaped carbon nanotubes (CNTs) intermingled in a porous carbon network. High-resolution transmission electron microscopy (HR-TEM) confirmed the presence of CNTs with distinct bamboo-like joints (Figure 4c,d), characteristic of nitrogen-doping in the carbon,[40,41] and revealed particles within some of the CNT compartments that could not be indexed as pure Fe or Fe_3C (Figure 4c–e). On the basis of these results, we believe the Fe is retained throughout the heat treatments and agglomerates into particles (metallic Fe NPs) in which the dissociated carbon and nitrogen diffuses through to form the witnessed CNTs.

Nitrogen-sorption analysis was performed to monitor the change of surface area and evolution of porosity throughout the synthetic process leading up to final formation of FePhen@MOF-ArNH$_3$. Brunauer-Emmet-Teller (BET) surface area of the as synthesized FePhen@MOF was measured and compared with a commercially available ZIF-8 MOF (Sigma, Basolite Z1200, similar MOF without the encapsulated chelated Fe-phenanthroline). The diminished surface area of FePhen@MOF in comparison to Basolite (Figure 5a) (424 m^2/g vs 1813 m^2/g) is ascribed to presence of the iron-phenanthroline complex encapsulated within the pores, causing a substantial reduction in the overall pore volume. However, the surface area increased significantly following the two heat treatments in argon and ammonia respectively, engendering FePhen@MOF-ArNH$_3$ with a BET surface area comparable to unheat treated Basolite (1200 m^2/g vs 1813 m^2/g). Using density functional theory (DFT) split pore method simulation (Figure 5b), the pore-size distribution of FePhen@MOF reveals its microporous arrangement (<20 Å) and narrow size distribution. A non-local density functional theory (NLDFT) model available within the analysis software was used in this case. Yet when subjected to the heat treatment process the pore size distribution is altered dramatically. The volume and size of micropores in FePhen@MOF-ArNH$_3$ increased in comparison to FePhen@MOF, and mesopores (20–40 Å) that were not originally present in FePhen@MOF were introduced following the heat treatments.

The presence of Fe in the synthesis of non-PGMs is essential to obtain the most active electrocatalysts,[42] but the role of Fe in ORR activity is ambiguous. X-ray absorption spectroscopy (XAS) is an element specific technique that allows us to probe the structural and electronic nature of the Fe in FePhen@MOF-ArNH$_3$. Using a specially designed spectro-electrochemical cell[43] we are able to collect spectra in situ, simulating operating conditions of a fuel cell, which further enhanced the sensitivity of the technique. Spectra were collected as a function of potential on an electrode in 0.1 M HClO$_4$ electrolyte saturated with either oxygen or nitrogen. Electrodes held at 0.3 V vs RHE are considered to be free of adsorbates and are representative of the catalyst structure with a clean surface.[43] Shown in Figure 6 are the Fourier Transform (FT) of the extended X-ray absorption fine structure spectra (EXAFS). Analysis up to the second shell was applied at the Fe K-edge of FePhen@MOF-ArNH$_3$ data at 0.3 V (fitting results summarized in Supporting Information Table S1). FePhen@MOF-ArNH$_3$ exhibits one dominant FT peak at ∼2.2 Å (without phase correction), which can be fit well with a Fe–Fe scattering path with a bond length of ∼2.51 Å. This corresponds well with the known Fe–Fe bond length in bulk iron (2.49 Å) and/or iron carbide (2.48 Å). A small shoulder off the main peak was accounted for with a Fe–C/N scattering path with a bond length of ∼1.96 Å. C and N cannot be distinguished by XAS as surrounding atoms, but based on our XRD results we suspect that iron carbide and iron nitride are both present. X-ray absorption near-edge structure (XANES) spectra are very sensitive to changes in the oxidation state of Fe, and become even more sensitive when coupled with our *in situ* technique. Previous studies of Fe-based non-PGMs (heat treatment of a pre-existing macrocycle FeTPP[43] and PVAG-Fe[44] prepared using precursors from a reactive polymer method) identified Fe–N_x active sites in which the Fe-ion is coordinated by nitrogen in the carbon scaffold. These studies revealed that a key feature of ORR which typically occurs on Fe–N_x active sites involves redox transition close to 0.9 V involving Fe^{2+}/Fe^{3+} (sweeping anodically). This is manifest in expected shift of the Fe K edge XANES associated with the oxidation state. As can be seen in Figure 6b, the Fe K-edge XANES of FePhen@MOF-ArNH$_3$ however remains unchanged as the potential is increased from 0.1 to 0.9 V vs RHE, indicating that the Fe is not redox active and FePhen@MOF-ArNH$_3$ is devoid of FeN_x active sites. This absence of exposed Fe in coordination with

DOI: 10.1021/acscatal.8b00390
ACS Catal. 2018, 8, 3833–3843

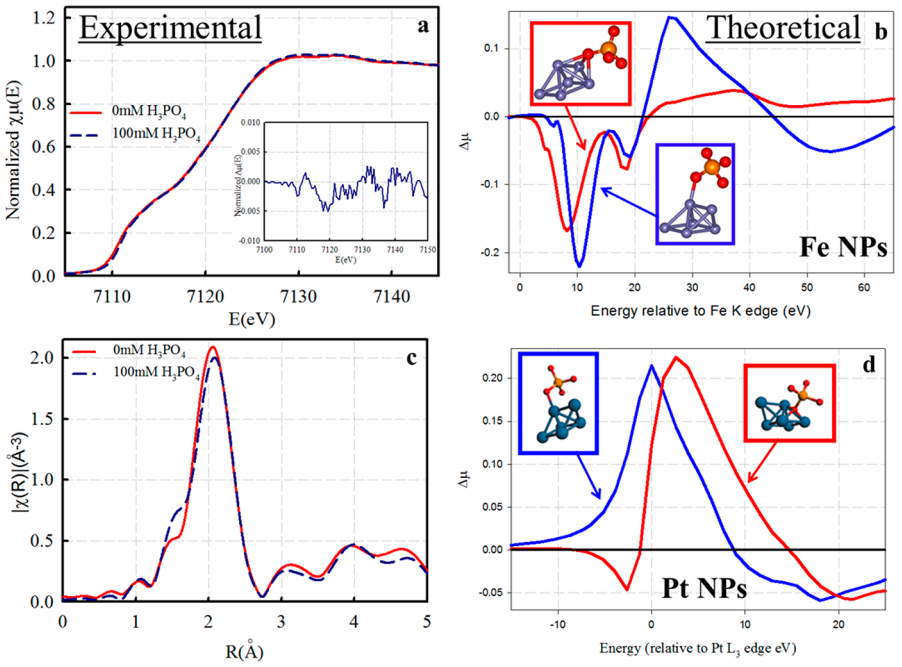

Figure 7. Anion Adsorption Investigation. (a) Fe K-edge XANES of FePhen@MOF-ArNH$_3$ at 0.3 V vs RHE in N_2 saturated 0.1 M $HClO_4$ with and without 100 mM H_3PO_4, with $\Delta\mu = \mu$ (0.9 V) - μ (0.3 V) (inset). (b) Theoretical $\Delta\mu$ signatures calculated by FEFF 8 of illustrated PO_4 adsorption on Fe_6 cluster. (c) Fourier Transform EXAFS of FePhen@MOF-ArNH$_3$ held at 0.3 V vs RHE in N_2 saturated 0.1 M $HClO_4$ with and without 100 mM H_3PO_4. (d) Theoretical $\Delta\mu$ signatures calculated by FEFF 8 of atop and fcc-inverted PO_4 adsorption on Pt_6 cluster.

nitrogen moieties undergoing redox transformation is typical in the vast majority of the such non PGM catalysts has an important connotation in the additional stability provided by the absence of any Fenton type reaction resulting from peroxide initiated free radical formation.[45] A recent report[44] from our group has clearly ascribed such redox transition and its importance within the context of the overall ORR mechanism to be predominant in active sites containing direct Fe−N coordination.

In summary, the above data indicates that the initial heat treatment of the FePhen@MOF synthesized via a chemical encapsulation method to a temperature above 550 °C results in the formation of a porous carbon framework as a result of the decomposition of the MOF structure and the evaporation of Zn. Subsequently, Fe agglomeration catalyzes the formation of carbon fibers as seen from the SEM and TEM micrographs. Subsequent heat treatment on NH_3 atmosphere engenders formation of the final catalyst with embedded Fe/Fe$_x$C/Fe$_x$N nanoparticles within the confines of carbo nitrided nanofibers. Our in situ XAS results confirm that FePhen@MOF-ArNH$_3$ is made up of metallic Fe particles and has no detectable Fe−N$_x$ moieties.

3.4. Delta Mu Anion Adsorption Investigation. Earlier radiotracer/FTIR study[20] on Pt-based electrodes have reported the potential dependence of $H_2PO_4^{2-}$ adsorption being governed by water displacement and oxide formation, resulting in adsorption well above the potential of zero charge (pzc). Most cathodic fuel cell reactions are initiated above the pzc and oxygen must compete with adsorbed species for access to the active site. Tanaka[19] et al., found that Pt-catalyzed ORR in concentrated phosphoric acid exhibits a structural sensitivity that originates from the 3-fold adsorption of the phosphate anion ($H_2PO_4^-$) on Pt(111) surface, but only a 1- or 2-fold adsorption on Pt(100) and Pt(110) surfaces. Their findings were corroborated by He[18] et al., who showed ORR on Pt single crystals was most severely poisoned on Pt(111) due to the abundance of 3-fold surface sites for phosphate anion adsorption. This was subsequently shown spectroscopically by our group[17] using in situ XAS spectroscopy at room temperature and by Roth's group[46] at elevated temperature with the aid of the subtractive method involving in in situ XANES referred to as Delta Mu technique. However, they found that poisoning was diminished when Pt (111) was alloyed with Sn by virtue of the steps and defects introduced on the PtSn(111) surface. A follow up study was conducted on a PtNi alloy in an attempt to mitigate phosphate anion poisoning by surface engineering.[17] Electrochemical and X-ray absorption spectroscopic (XAS) measurements determined poisoning of ORR was somewhat lower on PtNi/C as compared to Pt/C due to the changes in the nature of phosphate anion adsorption on PtNi/C (atop adsorption vs 3-fold site adsorption on Pt/C).

As mentioned above, some of the shortcomings of XAS spectroscopy, especially its bulk averaging character is overcome via the spectral subtraction method Delta Mu ($\Delta\mu$) applied to the XANES region.[29,30] The Fe K-edge XANES spectra in argon purged 0.1 M $HClO_4$ collected at 0.3 V was subtracted from spectra in the presence of 100 mM H_3PO_4 (Figure 7a) by applying the equation:

$$\Delta\mu = \mu(\mathrm{V, Ar100mM\,H_3PO_4}) - \mu(0.3\mathrm{V, Ar}) \quad (4)$$

to study the adsorbate coverage on the electrocatalyst surface. The adsorbate coverage on FePhen@MOF-ArNH$_3$ as a function of potential was monitored and the experimental $\Delta\mu$ spectrum (Figure 7a, inset) was compared with theoretical $\Delta\mu$ spectra generated from models (Figure 7b) representative of two different modes of phosphate anion adsorption on a Fe_6 cluster.[47] However, analysis of the experimental $\Delta\mu$ spectrum of FePhen@MOF-ArNH$_3$ revealed the $\Delta\mu$ amplitude ($|\Delta\mu|$) was within the noise range (<0.005 $|\Delta\mu|$) due to the lack of difference between the XANES spectra with and without

DOI: 10.1021/acscatal.8b00390
ACS Catal. 2018, 8, 3833−3843

H_3PO_4 (Figure 7a). Theoretical models predicted a $|\Delta\mu|$ of approximately 0.2 if the phosphate group was to interact with a Fe cluster. In a previously reported study of Fe-based non-PGMs, a $|\Delta\mu|$ of close to 0.4 was observed for changes on the Fe-surface associated with the interaction of the metal with oxygenated adsorbates.[44] As reported previously on studies of phosphate anion poisoning of Pt/C and PtNi/C electrocatalyst,[17] the surface changes observed from the interaction of the phosphate with the platinum metal produced a $|\Delta\mu|$ of 0.2, which is nearly an order of magnitude higher than the reliability threshold of 0.03 set for the Pt L_3-edge.[48] Combining these results with the microscopy imaging, we believe the Fe particles are located subsurface to graphitic layers and are protected from contact with electrolyte, therefore preventing phosphate anion adsorption. These findings further support our previous claim[21] on the absence of direct Fe−N coordination on the FePhen@MOF-Ar-NH_3 catalyst. As mentioned earlier the Fe configuration in FePhen@MOF-$ArNH_3$ has important implications for not only anion adsorption, but elimination of potential Fenton processes producing detrimental radicals. These results clearly show the FePhen@MOF-$ArNH_3$ catalyst is immune to phosphate adsorption at room temperature, which is likely related to its high performance in fuel cells. However, it is noted that the fuel cell testing was conducted at elevated temperature with concentrated phosphate anions that are harsher than the conditions wherein the immunity was detected in terms of phosphate poisoning. Therefore, the immunity of FePhen@MOF-$ArNH_3$ to phosphate adsorption needs to be examined under working conditions to ensure its contribution to the high fuel cell performance, especially considering a possible electrolyte structure changing at high phosphate concentrations that may modify phosphate adsorption on the non-PGM catalyst.[49] In situ XAS testing on the phosphate adsorption on Fe-based catalysts under elevated temperature and concentrated phosphate anions (which was previously done on Pt/C catalysts[46]), are under deliberation.

4. CONCLUSION

The effect of phosphate anion poisoning on a Fe-based non-PGM, FePhen@MOF-$ArNH_3$, was investigated electrochemically and spectroscopically. The results were compared with a state-of-the-art Pt-based ORR electrocatalyst using RDE. Additionally, the catalyst performance was evaluated for performance at 200 °C in single cell HT-PEMFC and demonstrating strong performance in both oxygen and air. As shown here, FePhen@MOF-$ArNH_3$ exhibits an almost complete immunity toward poisoning by phosphate anions (more specifically dihydrogen phosphate) at room temperature in contrast to typical noble-metal-supported electrocatalyst represented here by Pt/C/Low temperature RDE results in 0.1 M $HClO_4$ is supported by actual single cell MEA steady-state polarization results measured at 200 °C. Physicochemical studies show that FePhen@MOF-$ArNH_3$ comprises Fe/Fe_xC/Fe_xN particles embedded in graphitic carbon layers doped with nitrogen. In situ XAS results confirm that the Fe component of FePhen@MOF-$ArNH_3$ is metallic and subsurface, as indicated by the absence of oxidation state change of Fe with applied potential. Imaging with microscopy confirmed that the Fe particles are isolated from contact with electrolyte by graphitic layers that ultimately protect the Fe from adsorption of $H_2PO_4^-$. This was also confirmed by our poisoning studies using element specific in situ synchrotron XAS coupled with a surface sensitive subtractive technique. Comparison of experimental data with theoretical models revealed that phosphate anions introduced into the electrolyte do not interact with the Fe in FePhen@MOF-$ArNH_3$ at room temperature. On the basis of all the above physicochemical characterization results and our electrochemical investigation, we believe the Fe present in FePhen@MOF-$ArNH_3$ primarily acts as a catalyst for graphitization of the carbon during the synthesis. The ORR active site appears to be the carbon that is modified by N-doping and possibly subsurface Fe, participating through a synergistic effect. The presence of phosphate anions in the electrolyte has no detrimental effect on the ORR mechanism on the carbon-based active site.

■ ASSOCIATED CONTENT

Supporting Information

The Supporting Information is available free of charge on the ACS Publications website at DOI: 10.1021/acscatal.8b00390.

RDE polarization curves, phosphate anion poisoning Pt/C, Pt reference fuel cell polarization curves, X-ray absorption spectroscopy (XAS) analysis, EXAFS fits, and in situ EXAFS fit results (PDF)

■ AUTHOR INFORMATION

Corresponding Author

*E-mail: s.mukerjee@neu.edu. Phone: +1 617 373-2382.

ORCID

Ryan Pavlicek: 0000-0002-9229-5592
Qingying Jia: 0000-0002-4005-8894
Sanjeev Mukerjee: 0000-0002-2980-7655

Present Addresses

†E.M.: Department of Chemistry, Massachusetts Institute of Technology, 77 Massachusetts Avenue, Cambridge, Massachusetts 02139, United States

‡I.Z.: Visiting Researcher from School of Engineering, The University of Edinburgh, The King's Building, Mayfield Road, Edinburgh EH9 3JL, United Kingdom

Notes

The authors declare no competing financial interest.

■ ACKNOWLEDGMENTS

The authors thank The Department of Energy, EERE (DE-EE-0006965). Use of the synchrotron facilities at the National Synchrotron Light Source, beamlines X19A and X3B at Brookhaven National Laboratory, Upton, NY, is supported by the U.S. Department of Energy. This publication was made possible by the Center for Synchrotron Biosciences grant P30-EB-009998, from the National Institute of Biomedical Imaging and Bioengineering. Supports from beamline personnel Dr. Syed Khalid, Dr. Nebojsa Marinkovic, and Dr. Erik Farquhar are gratefully appreciated. Use of the Stanford Synchrotron Radiation Lightsource, SLAC National Accelerator Laboratory, is supported by the U.S. Department of Energy, Office of Science, Office of Basic Energy Sciences under Contract No. DE-AC02-76SF00515. Use of Beamline 2-2 at SSRL was partially supported by the National Synchrotron Light Source II, Brookhaven National Laboratory, under U.S. Department of Energy Contract No. DE-SC0012704.

DOI: 10.1021/acscatal.8b00390
ACS Catal. 2018, 8, 3833−3843

REFERENCES

(1) EG&G Technical Services, Inc. *Fuel Cell Handbook*, 7th ed.; U.S. Department of Energy, Office of Fossil Energy, National Energy Technology Laboratory: Morgantown, WV, 2004.

(2) Kunz, H. R. Lessons Learned from Phosphoric Acid Electrolyte Fuel Cell Development Pertinent to PEMFCs. *ECS Trans.* **2007**, *11* (1), 1447−1460.

(3) Appleby, A. J. Fuel cell technology: Status and future prospects. *Energy* **1996**, *21* (7), 521−653.

(4) Shao, Y.; Yin, G.; Wang, Z.; Gao, Y. Proton exchange membrane fuel cell from low temperature to high temperature: Material challenges. *J. Power Sources* **2007**, *167* (2), 235−242.

(5) Wainright, J. S.; Wang, J. T.; Weng, D.; Savinell, R. F.; Litt, M. Acid-Doped Polybenzimidazoles: A New Polymer Electrolyte. *J. Electrochem. Soc.* **1995**, *142* (7), L121−L123.

(6) Xiao, L.; Zhang, H.; Jana, T.; Scanlon, E.; Chen, R.; Choe, E. W.; Ramanathan, L. S.; Yu, S.; Benicewicz, B. C. Synthesis and Characterization of Pyridine-Based Polybenzimidazoles for High Temperature Polymer Electrolyte Membrane Fuel Cell Applications. *Fuel Cells* **2005**, *5* (2), 287−295.

(7) Quartarone, E.; Mustarelli, P. Polymer fuel cells based on polybenzimidazole/H3PO4. *Energy Environ. Sci.* **2012**, *5* (4), 6436−6444.

(8) Zhang, J.; Xie, Z.; Zhang, J.; Tang, Y.; Song, C.; Navessin, T.; Shi, Z.; Song, D.; Wang, H.; Wilkinson, D. P.; Liu, Z.-S.; Holdcroft, S. High temperature PEM fuel cells. *J. Power Sources* **2006**, *160* (2), 872−891.

(9) Li, Q.; Jensen, J. O.; Savinell, R. F.; Bjerrum, N. J. High temperature proton exchange membranes based on polybenzimidazoles for fuel cells. *Prog. Polym. Sci.* **2009**, *34* (5), 449−477.

(10) Samms, S.; Wasmus, S.; Savinell, R. Thermal stability of proton conducting acid doped polybenzimidazole in simulated fuel cell environments. *J. Electrochem. Soc.* **1996**, *143* (4), 1225−1232.

(11) Ma, Y.-L.; Wainright, J.; Litt, M.; Savinell, R. Conductivity of PBI membranes for high-temperature polymer electrolyte fuel cells. *J. Electrochem. Soc.* **2004**, *151* (1), A8−A16.

(12) Asensio, J. A.; Borrós, S.; Gómez-Romero, P. Proton-conducting polymers based on benzimidazoles and sulfonated benzimidazoles. *J. Polym. Sci., Part A: Polym. Chem.* **2002**, *40* (21), 3703−3710.

(13) Asensio, J. A.; Borrós, S.; Gómez-Romero, P. Polymer electrolyte fuel cells based on phosphoric acid-impregnated poly (2, 5-benzimidazole) membranes. *J. Electrochem. Soc.* **2004**, *151* (2), A304−A310.

(14) Kallitsis, J. K.; Geormezi, M.; Neophytides, S. G. Polymer electrolyte membranes for high-temperature fuel cells based on aromatic polyethers bearing pyridine units. *Polym. Int.* **2009**, *58* (11), 1226−1233.

(15) Pefkianakis, E. K.; Deimede, V.; Daletou, M. K.; Gourdoupi, N.; Kallitsis, J. K. Novel Polymer Electrolyte Membrane, Based on Pyridine Containing Poly (ether sulfone), for Application in High-Temperature Fuel Cells. *Macromol. Rapid Commun.* **2005**, *26* (21), 1724−1728.

(16) Papadimitriou, K. D.; Andreopoulou, A. K.; Kallitsis, J. K. Phosphonated fully aromatic polyethers for PEMFCs applications. *J. Polym. Sci., Part A: Polym. Chem.* **2010**, *48* (13), 2817−2827.

(17) He, Q.; Shyam, B.; Nishijima, M.; Ramaker, D.; Mukerjee, S. Mitigating Phosphate Anion Poisoning of Cathodic Pt/C Catalysts in Phosphoric Acid Fuel Cells. *J. Phys. Chem. C* **2013**, *117* (10), 4877−4887.

(18) He, Q.; Yang, X.; Chen, W.; Mukerjee, S.; Koel, B.; Chen, S. Influence of phosphate anion adsorption on the kinetics of oxygen electroreduction on low index Pt(hkl) single crystals. *Phys. Chem. Chem. Phys.* **2010**, *12* (39), 12544−12555.

(19) Tanaka, A.; Adzic, R.; Nikolic, B. Oxygen reduction on single crystal platinum electrodes in phosphoric acid solutions. *J. Serb. Chem. Soc.* **1999**, *64* (11), 695−705.

(20) Zelenay, P.; Habib, M.; Bockris, J. Adsorption from solution on platinum: an in situ FTIR and radiotracer study. *Langmuir* **1986**, *2* (4), 393−405.

(21) Strickland, K.; Miner, E.; Jia, Q.; Tylus, U.; Ramaswamy, N.; Liang, W.; Sougrati, M.-T.; Jaouen, F.; Mukerjee, S., Highly active oxygen reduction non-platinum group metal electrocatalyst without direct metal-nitrogen coordination. *Nat. Commun.* **2015**, *6*.Article No. 734310.1038/ncomms8343

(22) Jaouen, F. d. r.; Herranz, J.; Lefèvre, M.; Dodelet, J.-P.; Kramm, U. I.; Herrmann, I.; Bogdanoff, P.; Maruyama, J.; Nagaoka, T.; Garsuch, A.; Dahn, J. R.; Olson, T.; Pylypenko, S.; Atanassov, P.; Ustinov, E. A. Cross-Laboratory Experimental Study of Non-Noble-Metal Electrocatalysts for the Oxygen Reduction Reaction. *ACS Appl. Mater. Interfaces* **2009**, *1* (8), 1623−1639.

(23) Jaouen, F.; Proietti, E.; Lefevre, M.; Chenitz, R.; Dodelet, J.-P.; Wu, G.; Chung, H. T.; Johnston, C. M.; Zelenay, P. Recent advances in non-precious metal catalysis for oxygen-reduction reaction in polymer electrolyte fuel cells. *Energy Environ. Sci.* **2011**, *4* (1), 114−130.

(24) Tylus, U.; Mukerjee, S.; Miner, E.; Strickland, K. Non-noble metal catalysts for oxygen depolarized cathodes and their uses. US20150340705A1, 2014.

(25) Gojković, S. L.; Gupta, S.; Savinell, R. Heat-treated iron (III) tetramethoxyphenyl porphyrin chloride supported on high-area carbon as an electrocatalyst for oxygen reduction: Part II. Kinetics of oxygen reduction. *J. Electroanal. Chem.* **1999**, *462* (1), 63−72.

(26) Li, Q.; Wu, G.; Cullen, D. A.; More, K. L.; Mack, N. H.; Chung, H. T.; Zelenay, P. Phosphate-Tolerant Oxygen Reduction Catalysts. *ACS Catal.* **2014**, *4* (9), 3193−3200.

(27) Strickland, K.; Miner, E.; Mukerjee, S. *Resistance of Metal-Organic Framework Based ORR Catalysts to Phosphate Ion Adsorption*; Presented at the 224th Electrochemical Society Meeting, San Fransisco, CA, October 27−November 1, 2013; p 305.

(28) Strickland, K.; Mukerjee, S. In *Non-precious metal catalysts (NPMC): Investigating phosphate ion adsorption*; Abstracts of Papers of the American Chemical Society, Presented at the American Chemical Society National Meeting, Indianapolis, IN, September 8−12, 2013.

(29) Teliska, M.; O'Grady, W.; Ramaker, D. Determination of H adsorption sites on Pt/C electrodes in HClO4 from Pt L23 X-ray absorption spectroscopy. *J. Phys. Chem. B* **2004**, *108* (7), 2333−2344.

(30) Teliska, M.; O'Grady, W.; Ramaker, D. Determination of O and OH adsorption sites and coverage in situ on Pt electrodes from Pt L23 X-ray absorption spectroscopy. *J. Phys. Chem. B* **2005**, *109* (16), 8076−8084.

(31) Glass, J. T.; Cahen, G. L.; Stoner, G. E. The effect of phosphoric acid concentration on electrocatalysis. *J. Electrochem. Soc.* **1989**, *136* (3), 656−660.

(32) Arruda, T. M.; Shyam, B.; Lawton, J. S.; Ramaswamy, N.; Budil, D. E.; Ramaker, D. E.; Mukerjee, S. Fundamental Aspects of Spontaneous Cathodic Deposition of Ru onto Pt/C Electrocatalysts and Membranes under Direct Methanol Fuel Cell Operating Conditions: An in Situ X-ray Absorption Spectroscopy and Electron Spin Resonance Study. *J. Phys. Chem. C* **2010**, *114* (2), 1028−1040.

(33) Newville, M. IFEFFIT: interactive XAFS analysis and FEFF fitting. *J. Synchrotron Radiat.* **2001**, *8* (2), 322−324.

(34) Ravel, B.; Newville, M. ATHENA and ARTEMIS: interactive graphical data analysis using IFEFFIT. *Phys. Scr.* **2005**, *2005* (T115), 1007.

(35) Zabinsky, S. I.; Rehr, J. J.; Ankudinov, A.; Albers, R. C.; Eller, M. J. Multiple-scattering calculations of x-ray-absorption spectra. *Phys. Rev. B: Condens. Matter Mater. Phys.* **1995**, *52* (4), 2995−3009.

(36) Ankudinov, A.; Ravel, B.; Rehr, J.; Conradson, S. Real-space multiple-scattering calculation and interpretation of x-ray-absorption near-edge structure. *Phys. Rev. B: Condens. Matter Mater. Phys.* **1998**, *58* (12), 7565.

(37) Park, K. S.; Ni, Z.; Cote, A. P.; Choi, J. Y.; Huang, R.; Uribe-Romo, F. J.; Chae, H. K.; O'Keeffe, M.; Yaghi, O. M. Exceptional chemical and thermal stability of zeolitic imidazolate frameworks. *Proc. Natl. Acad. Sci. U. S. A.* **2006**, *103* (27), 10186.

(38) Jaouen, F.; Dodelet, J.-P. Non-Noble Electrocatalysts for O2 Reduction: How Does Heat Treatment Affect Their Activity and Structure? Part I. Model for Carbon Black Gasification by NH3:

DOI: 10.1021/acscatal.8b00390
ACS Catal. 2018, 8, 3833−3843

Parametric Calibration and Electrochemical Validation. *J. Phys. Chem. C* **2007**, *111* (16), 5963−5970.
(39) Figueiredo, J.; Pereira, M.; Freitas, M.; Orfao, J. Modification of the surface chemistry of activated carbons. *Carbon* **1999**, *37* (9), 1379−1389.
(40) Banks, C. E.; Davies, T. J.; Wildgoose, G. G.; Compton, R. G. Electrocatalysis at graphite and carbon nanotube modified electrodes: edge-plane sites and tube ends are the reactive sites. *Chem. Commun.* **2005**, *7*, 829−841.
(41) Maldonado, S.; Stevenson, K. J. Influence of Nitrogen Doping on Oxygen Reduction Electrocatalysis at Carbon Nanofiber Electrodes. *J. Phys. Chem. B* **2005**, *109* (10), 4707−4716.
(42) Zagal, J. H.; Bedioui, F.; Dodelet, J. P. N 4 -Macrocyclic Metal Complexes. *J. Am. Chem. Soc.* **2007**, *129*, 1471−1472.
(43) Ramaswamy, N.; Tylus, U.; Jia, Q.; Mukerjee, S. Activity Descriptor Identification for Oxygen Reduction on Nonprecious Electrocatalysts: Linking Surface Science to Coordination Chemistry. *J. Am. Chem. Soc.* **2013**, *135* (41), 15443−15449.
(44) Tylus, U.; Jia, Q.; Strickland, K.; Ramaswamy, N.; Serov, A.; Atanassov, P.; Mukerjee, S. Elucidating Oxygen Reduction Active Sites in Pyrolyzed Metal−Nitrogen Coordinated Non-Precious-Metal Electrocatalyst Systems. *J. Phys. Chem. C* **2014**, *118* (17), 8999−9008.
(45) Zhang, L.; Mukerjee, S. Investigation of durability issues of selected nonfluorinated proton exchange membranes for fuel cell application. *J. Electrochem. Soc.* **2006**, *153* (6), A1062−A1072.
(46) Kaserer, S.; Caldwell, K. M.; Ramaker, D. E.; Roth, C. Analyzing the Influence of H3PO4 as Catalyst Poison in High Temperature PEM Fuel Cells Using in-operando X-ray Absorption Spectroscopy. *J. Phys. Chem. C* **2013**, *117* (12), 6210−6217.
(47) Janin, E.; Von Schenck, H.; Göthelid, M.; Karlsson, U.; Svensson, M. Bridge-bonded atomic oxygen on Pt (110). *Phys. Rev. B: Condens. Matter Mater. Phys.* **2000**, *61* (19), 13144.
(48) Stoupin, S. Influence of Adsorbate-Free Atoms on Δ-XANES Signatures. *J. Chem. Theory Comput.* **2009**, *5* (5), 1337−1342.
(49) Zelenay, P. A Comparison of the Properties of CF[sub 3]SO[sub 3]H and H[sub 3]PO[sub 4] in Relation to Fuel Cells. *J. Electrochem. Soc.* **1986**, *133* (11), 2262.

DOI: 10.1021/acscatal.8b00390
ACS Catal. 2018, 8, 3833−3843